Journal of the Geological Society, London, Vol. **160**, 2003, pp. 299–308. Printed in Great Britain.

Sulphur isotope geochemistry of black shale-hosted antimony mineralization, Arnsberg, northern Rhenish Massif, Germany: implications for late-stage fluid flow during the Variscan orogeny

THOMAS WAGNER[1,2] & ADRIAN J. BOYCE[3]

[1]*Mineralogisches Institut, Universität Würzburg, Am Hubland, D-97074 Würzburg, Germany*

[2]*Department of Earth and Planetary Sciences, McGill University, 3450 University Street, Montréal H3A 2A7, Quebec, Canada (e-mail: wagner@eps.mcgill.ca)*

[3]*Scottish Universities Environmental Research Centre (SUERC), East Kilbride, Glasgow G75 0QF, UK*

Abstract: Vein-type and bedding-concordant mesothermal (180–410 °C) stibnite–sulphosalt mineralization at Arnsberg, NE Rhenish Massif, Germany, is hosted by Carboniferous pyrite-rich black shales and siliceous limestones. A detailed sulphur isotope study of the stibnite–sulphosalt mineralization and pyrite from a variety of regional host-rock lithologies has been carried out using an *in situ* laser combustion technique. The δ^{34}S values of stibnite of various textural types are distinctly negative and lie in a narrow range between −23.9‰ and −17.1‰ (mean −20.1‰). In contrast, regional sedimentary–diagenetic pyrites display a large variation of their δ^{34}S values between −45.4‰ and +9.3‰. There is little evidence for significant modification of the hydrothermal fluid during deposition and the S isotope signatures suggest that the sulphur of the stibnite mineralization was not locally derived. The δ^{34}S values of pyrite in Givetian shales display a significantly narrower range of −28.2‰ to −7.5‰ and their mean composition (−17.1‰) is close to the δ^{34}S values of the Arnsberg stibnite deposits. Considering the temperature-dependent isotopic fractionation between stibnite and reduced sulfur species, the δ^{34}S values of the mineralizing fluid (−16.8‰; 200 °C) and the Givetian rock source are essentially identical. Therefore, we propose a model of leaching and isotopic homogenization of sulphur from the Middle Devonian shales and a subsequent northward migration of these fluids. The fluids were trapped in permeability-controlled positions within anticlinal zones, where fluid cooling induced deposition of stibnite and sulphosalts.

Keywords: antimony deposits, black shales, sulphur, isotopes, fluid flow.

The understanding of crustal-scale fluid flow in collisional orogenic belts has benefited from a large number of studies carried out on various synorogenic mineralization styles. These mineralizations, notably quartz–Au– (Sb) veins, Pb–Zn veins and barren quartz veins, record critical information about synorogenic fluid flow in space and time. By applying geochemical, isotopic and fluid inclusion studies to these mineralizations, the fluid chemistry and the scale of fluid movements during orogenic processes can be reconstructed (e.g. Cox *et al*. 1986; Gray *et al*. 1991; Mullis *et al*. 1994; Pettke *et al*. 1999; Bierlein & Crowe 2000; Partington & Williams 2000; Barker *et al*. 2000; Oliver & Bons 2001). These datasets can, in turn, be used to substantially improve integrated dynamic models, accounting for changes of fluid flow and mass transfer rates during orogenic cycles. A key problem for such quantitative modelling of synorogenic fluid processes is the ultimate source of volatile and solute components contained in the hydrothermal fluids, which can be addressed by detailed isotopic studies of the mineralized structures and a broad range of potential source rocks (e.g. Pettke & Diamond 1997; Tosdal *et al*. 1999; Heinrich *et al*. 2000). Besides contributing to our understanding of mineralization processes, such isotopic case studies of metallogenic districts within orogenic belts are particularly useful for reconstructing the magnitude and dimension of synorogenic fluid convection systems.

Sediment-hosted vein-type stibnite deposits constitute a major type of mesothermal Sb–Au mineralization in most collisional orogenic belts, and are frequently located within black shale units of sedimentary sequences (e.g. Gumiel & Arribas 1987; Nesbitt *et al*. 1989; Ortega & Vindel 1995; Dill 1998). Several studies have focused on the genetic link between the black shales and the mesothermal Sb and Au deposits; black shales may serve as a potential source of metals and/or sulphur and as a dominant lithological–geochemical control of the ore deposition (e.g. Dill 1985; Bottrell & Spiro 1988; Guillemette & Williams-Jones 1993; Arias *et al*. 1997). Based on textural relationships and stable isotope evidence, the mobilization of the sulphur contained in vein sulphides from the host-rock black shales could be demonstrated for a number of cases (Guillemette & Williams-Jones 1993; Arias *et al*. 1997). In contrast, it was not possible to show a major contribution of the black shales to the metal inventory of the mesothermal vein-type mineralizations (e.g. Bottrell & Spiro 1988; Bottrell *et al*. 1988).

The present study reports the results of a detailed sulphur isotope investigation of bedding-concordant and vein-type Sb deposits and their host-rock black shales located at the northern margin of the fold–thrust belt of the Rhenohercynian zone in the German part of the European Variscides. This mineralization style represents a particular type of mesothermal Sb– (Au) mineralization, which is generally widespread in the central and western parts of the European Variscan orogen (e.g. Boiron *et al*. 1990; Munoz *et al*. 1992; Ortega & Vindel 1995; Clayton & Spiro 2000; Noronha *et al*. 2000). Previous work on Sb deposits in the Rhenohercynian zone has included studies of textural relationships, mineral chemistry, alteration geochemistry and fluid inclusion characteristics (Wagner & Cook 2000). Our

sulphur isotope investigation has focused on the following objectives: (1) characterization of the sulphur isotope composition of the mineralized structures; (2) detailed analysis of various textural types of pyrite within the black shales; (3) assessment of the sulphur isotope effect of fluid–rock interaction; (4) identification of the potential sulphur source. The results of our studies show that the Sb mineralization is characterized by distinctly negative and restricted $\delta^{34}S$ values, whereas the host-rock black shales display extremely variable sulphur isotope compositions, which makes a local derivation of the sulphur improbable. Evaluation of our data within the framework of available S isotope datasets from various sedimentary rock sequences points to 10–20 km lateral fluid migration to the northern margin of the Rhenohercynian fold–thrust belt.

Regional geology

The fold–thrust belt of the Rhenish Massif forms a part of the northern external zone (Rhenohercynian) of the Central European Variscan orogen. It is composed of marine Lower Devonian to Upper Carboniferous (volcano)-sedimentary rock sequences (pelitic to psammitic siliciclastic sediments, acidic and basic volcaniclastic rocks, carbonates and black shales), which were deposited in the Rhenohercynian basin. Activation of the continental margin of the Mid-German Crystalline Rise resulted in south-directed subduction in early Late Devonian time and the accretion of shelf sediments during Early Carboniferous time (Franke & Oncken 1990). The (volcano)-sedimentary sequences were deformed under predominantly SE-directed compression, resulting in a SW–NE strike of the major structural units, including fold axes, the pervasive S_1 foliation and the major thrust systems (Oncken 1984, 1988). The deformational front progressed from south to north; peak metamorphic ages range from 327–318 Ma in the south to 305–290 Ma at the northern margin (Ahrendt *et al*. 1983). Metamorphic conditions have generally not exceeded very low grade, with peak metamorphic temperatures in the range of 180–320 °C (Oncken 1991; Dittmar *et al*. 1994). Late-orogenic evolution is characterized by the transition from compressional to extensional conditions, related to the Late Palaeozoic strike-slip regime in Central Europe (Arthaud & Matte 1977; Henk 1995).

The northern margin of the fold–thrust belt is composed of sedimentary sequences of Middle to Upper Devonian and Carboniferous rocks (Fig. 1). The Middle and Upper Devonian sedimentary units are characterized by very complex lithological and facies relationships, related to the evolution of large carbonate platforms (e.g. the Brilon complex) and the onset of an intense submarine bimodal volcanism. In the transition from Late Devonian to Early Carboniferous time, the extinction of the carbonate complexes and a significant shift to shale-dominated sedimentation occurred, related to the evolution of the Culm basin. As a consequence, the uppermost Devonian and Lower Carboniferous sediments are dominantly composed of black shales, siliceous shales and bituminous–siliceous limestones, with only minor intercalations of sandy shales. The Lower Carboniferous and lowermost Upper Carboniferous stratigraphic sequence is composed of the Culm siliceous shales, the Culm siliceous limestones, the Culm limestones and the upper black shales (Fig. 2). The upper black shales, which are the host rocks of most of the Sb mineralizations, are dominated in the upper part by pyrite-rich black shales with intercalations of fossil-rich layers (*Posidonia becheri*). The remainder of Late Carboniferous time was characterized by intense clastic sedimentation (turbiditic sandstones and greywackes of the Arnsberg Beds) and the subsequent evolution of paralic conditions, related to the accretionary tectonics in the southern part of the orogenic belt. The major folding of the northern margin of the Rhenohercynian occurred in latest Carboniferous time (Ahrendt *et al*. 1983; Büker *et al*. 1995).

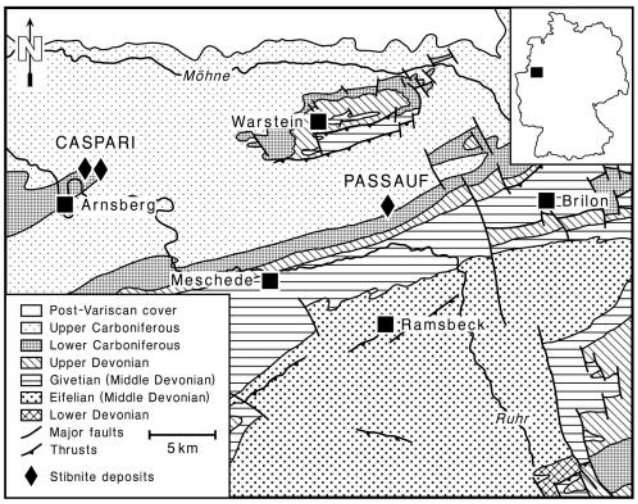

Fig. 1. Geological sketch map of the northern part of the Rhenish Massif, showing the location of the black shale-hosted antimony mineralizations. Redrawn and modified after Clausen *et al*. (1981).

Black shale-hosted antimony mineralization

Antimony mineralizations and host-rock black shales have been sampled at the Caspari (Arnsberg; Fig. 3) and Passauf (Nuttlar; Fig. 1) mines as well as at surface exposures at Bockstall (Arnsberg; Fig. 3), located 2 km WNW of the Caspari deposit. Additional samples were taken from various pyrite-rich layers of the black shale sequence (Fig. 3). The black shale-hosted antimony mineralizations are structurally situated at the flanks of major anticlinal zones, predominantly in close vicinity to significant lithological contrasts between siliceous–bituminous limestones and black shales. The antimony mineralizations in the Arnsberg area are hosted by the upper black shales and the uppermost portions of the underlying Culm limestones, whereas the Sb veins of the Passauf mine occur within a unit of siliceous black shales intercalated with the upper black shales. All antimony deposits are characterized by a comparatively simple mineralogy, which essentially comprises stibnite and minor amounts of quartz, pyrite, sphalerite, zinkenite ($Pb_9Sb_{22}S_{42}$), plagionite ($Pb_5Sb_8S_{17}$) and semseyite ($Pb_9Sb_8S_{21}$). Most of the stibnite ores of the Caspari deposit occur within the upper black shales as bedding-concordant mineralizations, which form massive layers and lenses of 5–15 cm thickness preferentially concentrated along reopened bedding planes. The bedding-concordant ores are commonly associated with dispersed impregnations of stibnite within the host-rock black shales. In addition to the massive ores, several extension veins carrying a quartz–stibnite–sulphosalt assemblage are also present. Antimony mineralization at Bockstall comprises several extension veins of fibrous stibnite, 2–8 cm in thickness. The black shales hosting the extension veins are impregnated with stibnite crystals, the amount of stibnite decreasing with distance from the veins. The Sb mineralization of the Passauf deposit forms a network of numerous quartz–stibnite veinlets, 5 mm to 2 cm in thickness, which crosscut siliceous black shales. Wallrock alteration related

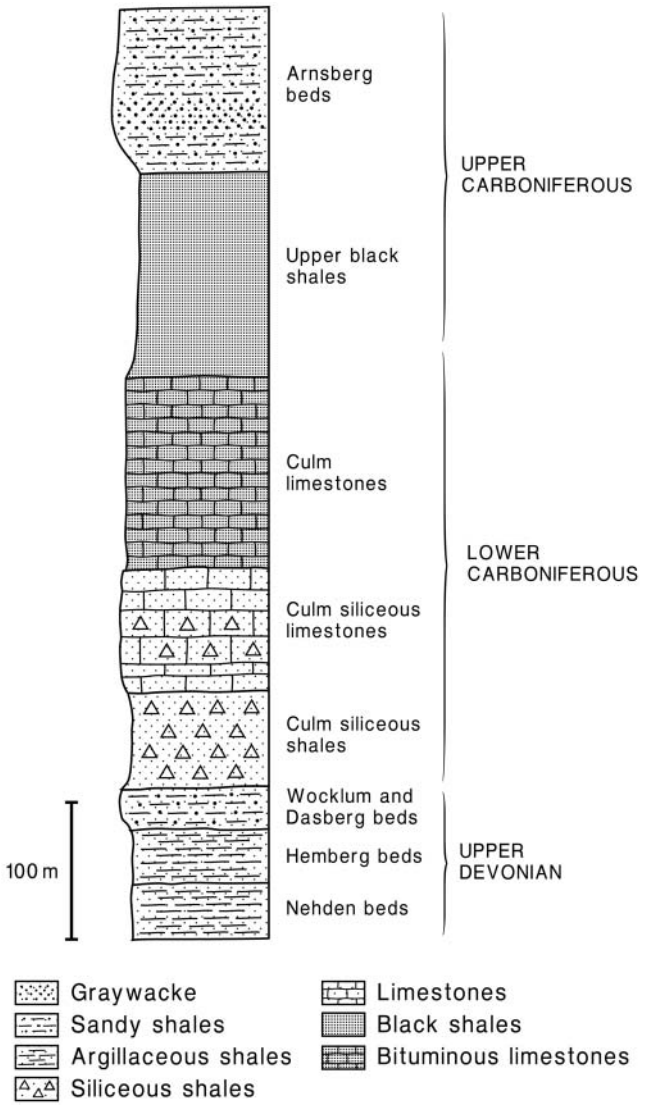

Fig. 2. Schematic stratigraphic section through the black shale sequence at the transition between Upper Devonian and Carboniferous units in the northern Sauerland, based on a compilation of available data (Kühne 1938*a*, *b*; Clausen *et al*. 1981; Clausen 1984; Clausen & Leuteritz 1984).

to the Sb mineralization is generally not pronounced; black shales in contact with the Sb ores display a darker colour, resulting from a local increase in coalification of organic matter in the shales.

Mineralogy and textures

The textural relationships of a representative suite of samples of the Sb mineralizations and pyrite-rich layers of the black shale units hosting the mineralizations have been studied in detail; a description of the respective samples is given in Table 1. The extension veins exposed at Bockstall display a typical fibrous texture composed of subparallel-intergrown stibnite crystals (Fig. 4a), which is similar to syntaxial fibrous quartz veins (Ramsay & Huber 1987). Very commonly, the central portions of these veinlets have been filled by much smaller prismatic stibnite needles, acicular zinkenite and minor amounts of quartz. The fibrous stibnite veins crosscut the host-rock black shales with

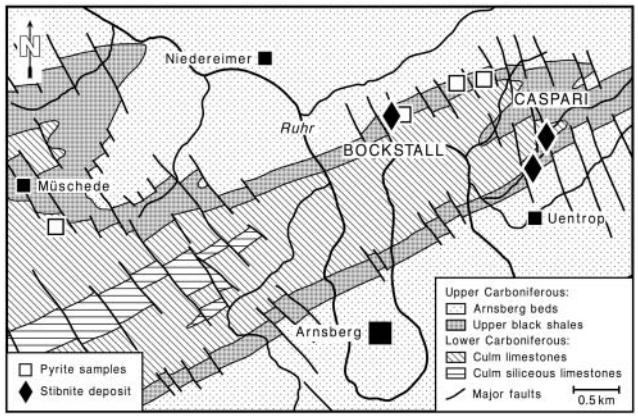

Fig. 3. Detailed geological map of the Arnsberg anticline, showing the location of the sampled antimony deposits and black shales. Redrawn after Kühne (1938*a*, *b*).

sharp contacts and the vein walls are frequently coated with dark organic material. A 5–10 cm wide zone of the black shales close to the veinlets is impregnated with prismatic and acicular stibnite crystals of 100 μm to 1.5 cm size, which show very irregular grain boundaries (Fig. 4b). Both the amount of stibnite impregnation and the average size of the crystals decrease with distance from the extension veins. Very commonly, the stibnite crystals enclose sedimentary pyrite, which is present as clusters of small crystals and framboids. Texturally similar sedimentary pyrites are also found in portions of the black shale samples, where almost no stibnite impregnation is detectable.

Bedding-concordant Sb mineralization, which constitutes the dominant mineralization style of the Caspari mine, is present as layers and lenses composed of elongated prismatic and blocky stibnite crystals, which are oriented parallel to the bedding of the host-rock black shales. The contacts to the black shale are very irregular and the black shale close to the massive bedding-concordant lenses displays an impregnation with radial groups of acicular to prismatic stibnite crystals. The cleavage planes between prismatic stibnite crystals have been infilled by sphalerite (Fig. 4c). In addition to the bedding-concordant mineralization, numerous quartz–stibnite–sulphosalt extension veins are also present. They are dominantly composed of syntaxial fibrous quartz, which has been subsequently overgrown by stibnite, zinkenite and sphalerite.

The textural relationships of the Sb mineralization found at the Passauf mine are very similar to those of the Caspari extension veins. A network of numerous quartz–stibnite veinlets crosscuts the siliceous black shale with sharp vein contacts. Very commonly, the central portions of the quartz veinlets show fissures and open vugs, which have been dominantly filled by stibnite (Fig. 4d), whereas only minor amounts of zinkenite and sphalerite are present.

Pyrite-rich layers of the black shales and bituminous limestones show a large variety of pyrite microtextures. Framboidal pyrite is present in most of the samples, most commonly in close association with pyrite crystals of varying shape and size. The framboidal pyrite forms either individual framboids intergrown with minute crystals of pyrite or composite aggregates, composed of several round bodies with smaller framboids distributed interstitially between these bodies (Fig. 5a). In addition, framboidal pyrite can also be found as irregular elongated clusters or layers, which occur with idiomorphic crystals of pyrite (Fig. 5b). These pyrite crystals, which are 0.5–2 mm in size, have

Table 1. *Description of the investigated samples of black shale-hosted antimony mineralization*

Sample	Location	Mineralization style and textural relationships
BOC-1	Bockstall	Extension vein; fibrous stibnite and trace amounts of zinkenite
BOC-2	Bockstall	Extension vein; fibrous stibnite and trace amounts of zinkenite
BOC-3	Bockstall	Black shale (upper black shales); impregnation by prismatic–acicular stibnite crystals
BOC-4	Bockstall	Black shale (upper black shales); impregnation by prismatic–acicular stibnite crystals
BOC-5	700 m NE Bockstall	Black shale (upper black shales); pyrite-rich layer with framboids and small crystals
BOC-6	850 m NE Bockstall	Black shale (upper black shales); pyrite-rich layer with large crystals and framboids
CAS-1	Caspari mine, Glückauf level	Black shale (upper black shales); impregnation by prismatic stibnite crystals
CAS-2	Caspari mine, Maria level	Bedding-concordant mineralization; zinkenite with minor amounts of stibnite–sphalerite
CAS-3	Caspari mine	Bedding-concordant mineralization; contact between massive stibnite and black shale
CAS-4	Caspari mine	Extension vein; aggregate of prismatic and acicular stibnite crystals with minor sphalerite
MÜS-1a	Müschede quarry	Bituminous limestone (Culm limestones); pyrite-rich layer with centimetre-sized concretions
MÜS-1b	Müschede quarry	Bituminous limestone (Culm limestones); pyrite-rich layer with crystals and framboids
MÜS-2	Müschede quarry	Bituminous limestone (Culm limestones); pyrite-rich layer with centimetre-sized concretions
MÜS-3	Müschede quarry	Bituminous limestone (Culm limestones); pyrite-rich layer with crystals
PAS-2	Passauf mine, upper level	Extension vein; millimetre-thick quartz–stibnite veinlets in siliceous black shale

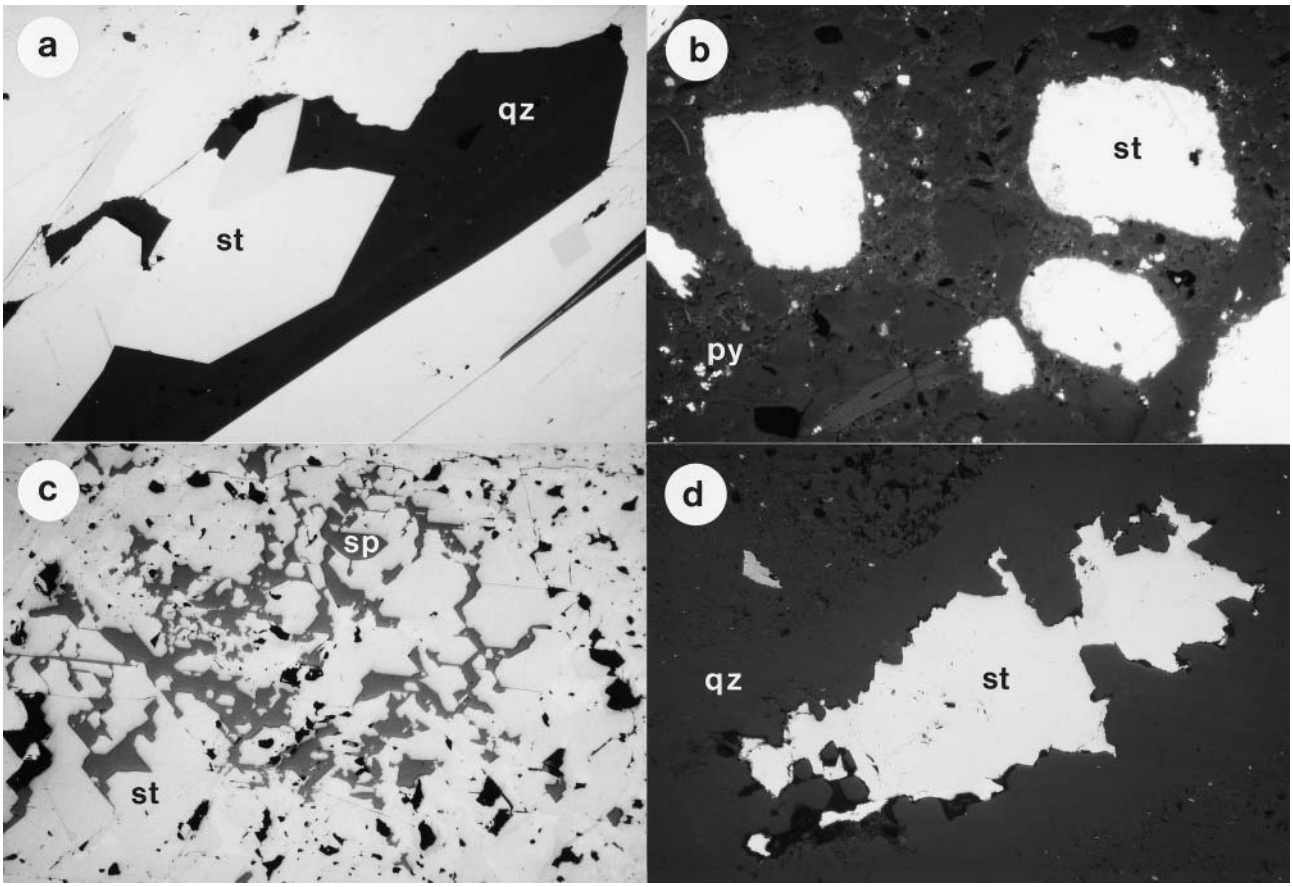

Fig. 4. Photomicrographs in reflected light, displaying various representative textures of the principal types of antimony mineralization. (**a**) Subparallel-intergrown fibrous stibnite (st) crystals in an extensional vein; Bockstall. Sample BOC-1. Width of field 1.50 mm. (**b**) Impregnation of anhedral stibnite grains in Upper Carboniferous black shale exposed in close spatial relationship to the extensional stibnite veins. The black shale contains numerous framboidal aggregates of pyrite (py); Bockstall. Sample BOC-4. Width of field 980 μm. (**c**) Massive stibnite from bedding-concordant mineralization. Fe-poor sphalerite (sp) has infilled along cleavage planes between stibnite crystals; Caspari. Sample CAS-3. Width of field 840 μm. (**d**) Portion of a quartz–stibnite veinlet hosted by upper Carboniferous siliceous shales. The open space in the quartz (qz) veinlet has been overgrown by anhedral stibnite; Passauf (Nuttlar) deposit. Sample PAS-2. Width of field 2.98 mm.

numerous inclusions of quartz and calcite. Most of the pyrite-rich black shales show elongated groups and layers of pyrite, which are composed of intimately intergrown framboids and numerous minute crystals with sharp crystal faces (Fig. 5c). Pyrite-rich layers of the bituminous–siliceous limestones are dominantly composed of elongated centimetre-sized pyrite clusters, which are arranged as groups of three or more individual clusters. The clusters are made up of composite inclusion-rich pyrite crystals (Fig. 5d) and are commonly associated with numerous individual pyrite crystals and framboids. In contrast to the large pyrite crystals present within the black shales, the composite pyrite crystals show relatively sharp crystal faces.

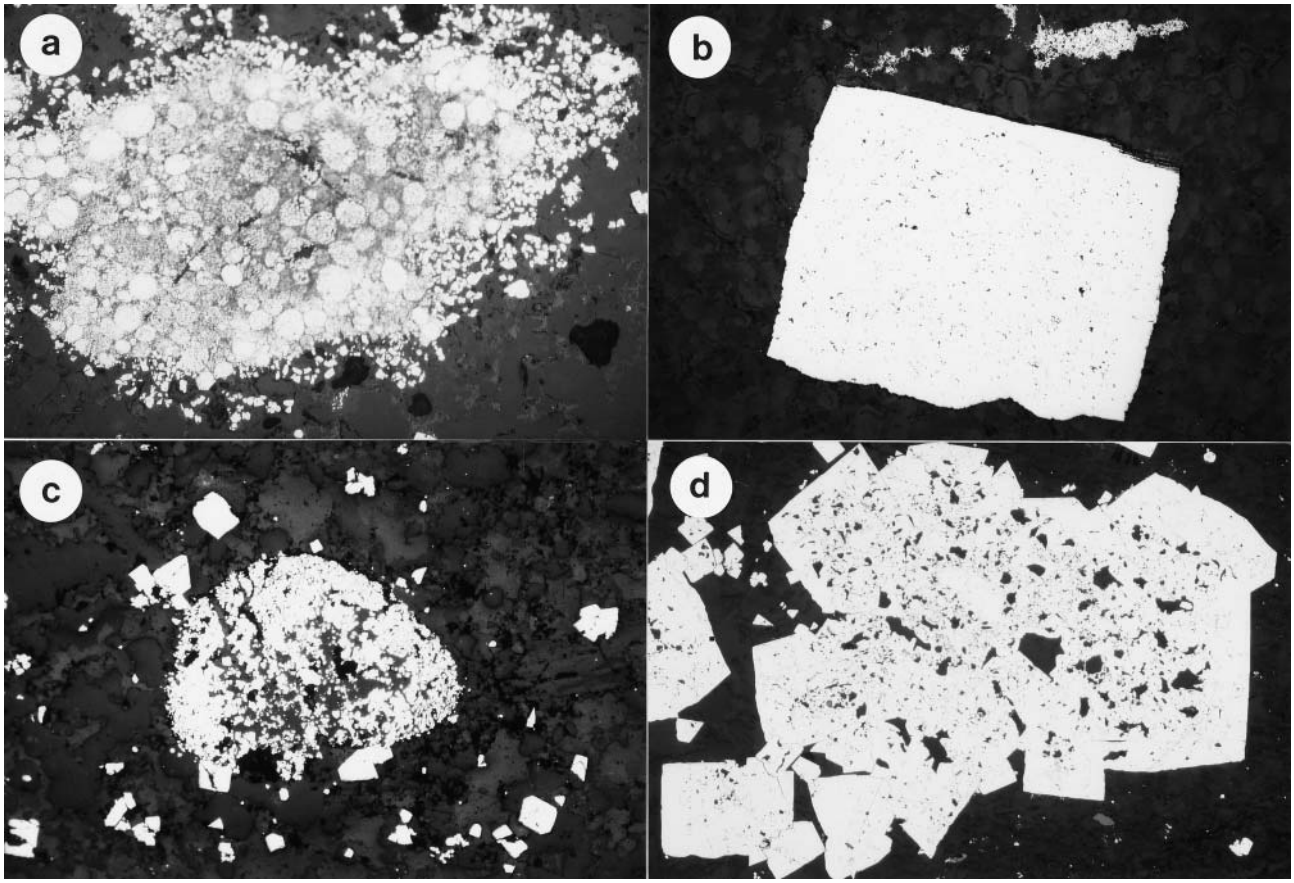

Fig. 5. Photomicrographs in reflected light, showing representative pyrite textures of the black shale units studied. (**a**) Composite framboidal aggregate of pyrite in Upper Carboniferous black shale hosting stibnite impregnations; Bockstall. Sample BOC-4. Width of field 900 μm. (**b**) Idiomorphic pyrite crystal associated with framboidal pyrite in Upper Carboniferous black shale; Arnsberg. Sample BOC-6. Width of field 1.57 mm. (**c**) Framboidal pyrite associated with small crystals of pyrite in Upper Carboniferous black shale; Arnsberg. Sample BOC-5. Width of field 1.0 mm. (**d**) Cluster of pyrite crystals in bituminous limestone (Culm limestones); Müschede quarry. Sample MÜS-1a. Width of field 2.17 mm.

Sulphur isotope data

Experimental procedures

Sulphur isotope analyses were carried out in the stable isotope laboratory at SUERC. Most of the samples were analysed by *in situ* laser combustion from standard polished blocks. The polished blocks were inserted into a sample chamber, which was evacuated and subsequently filled with an excess of oxygen gas (Fallick *et al*. 1992). Typically, a spot area of *c*. 300–400 μm diameter of the sulphide minerals was combusted using a Spectron Lasers 902Q CW Nd:YAG laser (1 W power), operating in TEM_{00} mode. The released SO_2 gas was purified in a vacuum line, which operates similar to a conventional sulphur extraction line (Kelley & Fallick 1990). The spatial resolution is determined by the minimum volume of SO_2 gas required for analysis (0.05–0.10 μmol), resulting in minimum spot sizes of *c*. 50–100 μm. Because of the small grain size of pyrite framboids and crystals in some of the black shale samples, cumulative analyses of 10–20 grains were carried out. SO_2 gas was produced from three stibnite separates using conventional combustion procedures (Robinson & Kusakabe 1975). Determination of the sulphur isotope composition of the purified SO_2 gas ($\delta^{66}SO_2$) was carried out on-line by a VG SIRA II gas source mass spectrometer. Reproducibility of the analytical results was monitored through replicate measurements of international standards NBS-123 (+17.1‰) and IAEA-S-3 (−31‰), as well as SUERC's internal laboratory standard CP-1 (−4.6‰). The analytical precision, based on replicate analyses of the standards, was around ±0.2‰ for both conventional and laser data. All sulphur isotope compositions were calculated relative to Vienna Cañon Diablo Troilite (V-CDT), and are reported in standard notation. The laser extraction method results in a sulphur isotope fractionation between the host mineral and the SO_2 gas produced via combustion, which is mineral-specific (Kelley & Fallick 1990). Experimentally determined fractionation factors are currently available in the SUERC system for several sulphide or sulphosalt minerals, including pyrite (+0.8‰) and stibnite (−1.2‰). The correction factor for zinkenite (+0.5‰) has been interpolated from the linear relationship between the laser fractionation and the molar fraction of PbS established in the Sb_2S_3–PbS system (Wagner *et al*. 2002).

Analytical results

Table 2 lists both gas and mineral $\delta^{34}S$ values for the studied Sb mineralizations and sediment-hosted pyrites. The sulphur isotope composition of stibnite of the various textural types is characterized by distinctly negative and restricted $\delta^{34}S$ values between −23.9‰ and −17.1‰ (Table 2; Fig. 6a); the mean of all the data is -20.1 ± 1.8‰ (1σ). All analysed stibnite samples from the Arnsberg area (Caspari and Bockstall) display an even more narrow range of $\delta^{34}S$ values of −21.3‰ to −17.1‰; their mean

Table 2. *Sulphur isotope data of Sb mineralization and sedimentary pyrites;* $\delta^{34}S_{mineral} = \delta^{34}S_{gas} + correction\ factor$

Sample	Mineral	Textural type	$\delta^{34}S_{V\text{-}CDT}$ (‰) (gas)	$\delta^{34}S_{V\text{-}CDT}$ (‰) (mineral)
BOC 1-1	Stibnite	Fibrous extension vein, margin	−19.8	−21.0
BOC 1-2	Stibnite	Fibrous extension vein, centre	−19.1	−20.3
BOC 2-1	Stibnite	Fibrous extension vein	−19.1	−20.3
BOC 3-1	Stibnite	Impregnation in black shale	−15.9	−17.1
BOC 3-3	Stibnite	Impregnation in black shale	−17.5	−18.7
BOC 3-5	Stibnite	Impregnation in black shale	−18.5	−19.7
BOC 3-7	Stibnite	Impregnation in black shale	−19.6	−20.8
BOC 4-1	Sibnite	Impregnation in black shale	−17.0	−18.2
CAS 1-2	Stibnite	Impregnation in black shale	−20.1	−21.3
CAS 1-3	Stibnite	Impregnation in black shale	−19.8	−21.0
CAS 2-1	Zinkenite	Massive veinlet	−20.8	−20.3
CAS 2-3	Zinkenite	Massive veinlet	−18.7	−18.2
CAS 3-A	Stibnite	Bedding-concordant ore		−18.5
CAS 4-A	Stibnite	Massive veinlet in black shale		−19.1
CAS 4-B	Stibnite	Massive veinlet in black shale		−19.5
PAS 2-1	Stibnite	Veinlet in siliceous shale	−22.4	−23.6
PAS 2-2	Stibnite	Veinlet in siliceous shale	−22.7	−23.9
BOC 3-6	Pyrite	Several framboids	−4.8	−4.0
BOC 4-2	Pyrite	Composite framboid	−4.9	−4.1
BOC 5-1	Pyrite	Small crystals + framboids	−13.8	−13.0
BOC 5-2	Pyrite	Small crystals + framboids	−13.3	−12.5
BOC 5-3	Pyrite	Aggregate of small crystals	−12.8	−12.0
BOC 6-1	Pyrite	Idiomorphic crystal, core	−21.1	−20.3
BOC 6-2	Pyrite	Idiomorphic crystal, rim	−20.5	−19.7
BOC 6-3	Pyrite	Idiomorphic crystal	−20.9	−20.1
BOC 6-4	Pyrite	Idiomorphic crystal	−21.5	−20.7
MÜS 1a-1	Pyrite	Cluster of idiomorphic crystals	−2.4	−1.6
MÜS 1a-2	Pyrite	Cluster of idiomorphic crystals	−3.4	−2.6
MÜS 1b-1	Pyrite	Several framboids	−2.2	−1.4
MÜS 1b-2	Pyrite	Cluster of idiomorphic crystals	−9.4	−8.6
MÜS 2-1	Pyrite	Cluster of idiomorphic crystals	−3.5	−2.7
MÜS 2-2	Pyrite	Idiomorphic crystal	−2.1	−1.3
MÜS 3-1	Pyrite	Several framboids	−1.3	−0.5
MÜS 3-2	Pyrite	Idiomorphic crystals	+8.5	+9.3

value including two zinkenite samples is -19.7 ± 1.2‰ (1σ). The two analysed stibnites from the Passauf mine have slightly more negative $\delta^{34}S$ values of −23.9‰ and −23.6‰, which are in any case close to the range of Sb mineralization in the Arnsberg area. Zinkenite, which has formed subsequent to the stibnite, has sulphur isotope compositions essentially identical to stibnite ($\delta^{34}S$ of −20.3‰ and −18.2‰). There is no systematic difference detectable between bedding-concordant and vein-type mineralizations; the compositional ranges of both types are essentially identical.

In contrast, sedimentary pyrites from both black shales and bituminous limestones show a significant variability of their $\delta^{34}S$ values in the range between −20.7‰ and +9.3‰, when compared with the stibnite mineralizations (Fig. 6b). The analysed compositional range of the pyrites overlaps with the sulphur isotope compositions of the Sb mineralizations, but most of the pyrite $\delta^{34}S$ values are significantly higher than those of the stibnites. Only one black shale sample with relatively large idiomorphic pyrite crystals (BOC-6) has $\delta^{34}S$ values in the range between −20.7‰ and −19.7‰, which are similar to the stibnite compositions. Framboidal pyrite and small pyrite crystals analysed in samples with considerable stibnite mineralization have $\delta^{34}S$ values of −4.1‰ and −4.0‰, which contrast markedly with stibnite compositions in the range between −20.8‰ and −17.1‰. The bituminous limestones have somewhat less negative sulphur isotope compositions ($\delta^{34}S$ of −8.6‰ to +9.3‰) than the black shale pyrites ($\delta^{34}S$ of −20.7‰ to −4.0‰). This may be related to the presence of relatively large, probably late-diagenetic pyrite clusters in the bituminous limestones, whereas smaller framboids and crystals predominate in the black shales. Koch (1993) has analysed bulk pyrite concentrates from various types of C_{org}-rich sediments in the Rhenish Massif. Compared with sulphur isotope data for bulk pyrite samples from Lower Carboniferous black shale units in the northeastern part of the Sauerland area (Fig. 6c), the $\delta^{34}S$ values of host-rock pyrites in both the black shales and bituminous limestones in the Arnsberg area (Fig. 6b) are generally higher.

Discussion

Isotope variation

Following characterization of the sulphur isotope composition of both stibnite ores and pyrites in various black shale units, the potential sulphur sources for the antimony mineralization can be evaluated, using the framework of available geological and mineralogical–geochemical data. The sulphur isotope composition of hydrothermal sulphide minerals is essentially controlled by (1) the isotopic composition of the fluid, (2) temperature, (3) the amount of sulphide minerals deposited from the fluid, and (4) the fO_2–pH conditions of the fluid (Ohmoto 1972; Ohmoto & Rye 1979; Ohmoto & Goldhaber 1997). Only the initial isotopic composition of the fluid is characteristic of the source, whereas evolution of the fluid in the depositional environment can result

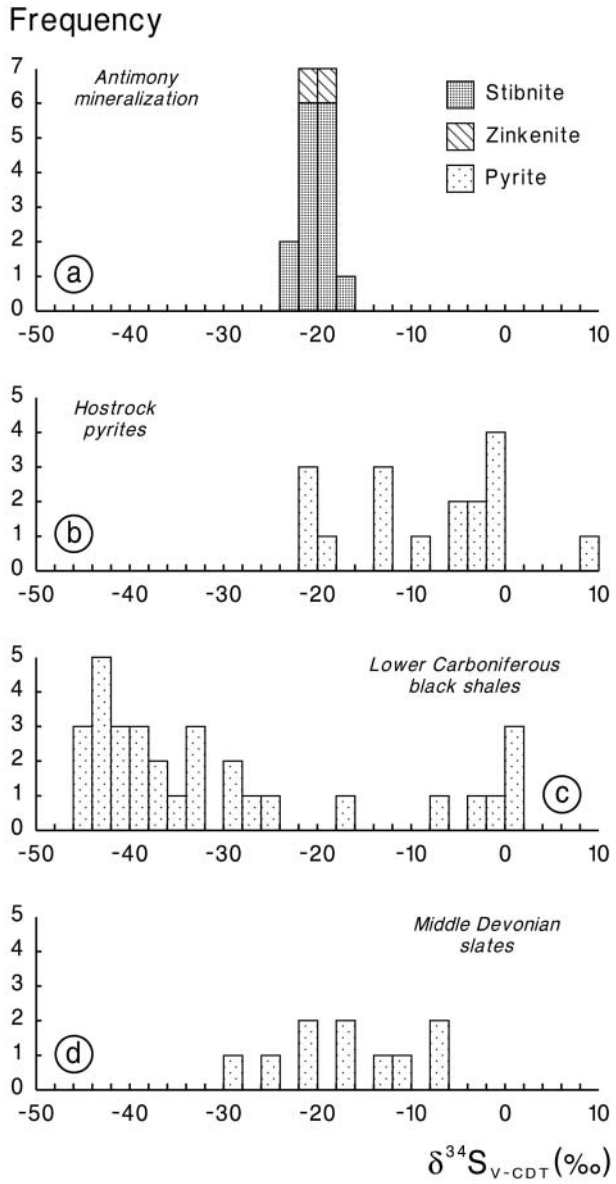

Fig. 6. Histograms displaying the sulphur isotope compositions of black shale-hosted antimony mineralization compared with the pyrite composition of various potential source rocks. (**a**) Stibnite and zinkenite from all types of mineralization investigated (extension veins, bedding-concordant mineralization, impregnations). (**b**) Pyrite from mineralized and non-mineralized black shales and bituminous limestones. (**c**) Bulk pyrite concentrates of C_{org}-rich Carboniferous siliceous shales, siliceous limestones and black shales. (**d**) Bulk pyrite concentrates of Middle Devonian slates. Data for (**c**) and (**d**) from Koch (1993).

in significant modification of the physico-chemical parameters and, consequently, the sulphur isotope composition of the precipitated sulphide minerals. Sulphide-dominated, reduced fluids will yield more restricted isotopic inter-mineral and mineral–fluid variation, whereas much greater variation is observed in more oxidized systems involving SO_2 and SO_4 as well as sulphide (Ohmoto 1972). In the reduced systems, mineral $\delta^{34}S$ is close to the fluid $\delta^{34}S$, whereas in the latter system, fluid $\delta^{34}S$ can be very different from mineral $\delta^{34}S$ (Rye 1993). The stibnite-dominated assemblage is relatively reduced (see discussion of fO_2–pH conditions below) and so we would not anticipate, and do not observe, large isotopic variation. Calculation of the sulphur isotope effect of variations in physico-chemical conditions of the hydrothermal fluids at the depositional site requires reasonable temperature constraints from either mineral geothermometry or fluid inclusion studies. Microthermometric studies carried out on quartz–stibnite–sulphosalt extension veins from the Caspari and Passauf mines demonstrate that high-temperature low-salinity (3.9–11.0 wt% equivalent NaCl) H_2O–NaCl–KCl fluids were responsible for antimony mineralization. The calculated model P–T conditions at the onset of mineralization are 380–410 °C at 0.2–0.4 kbar. Significant fluid cooling resulted in minimum temperatures of 150–220 °C during the late stage of fibrous quartz growth, which coincides with the stage of stibnite formation within the quartz–stibnite–sulphosalt veinlets (Wagner & Cook 2000).

Rayleigh fractionation

The sulphur isotope composition of minerals precipitated from hydrothermal fluids can be most effectively modified via Rayleigh fractionation or through significant changes of the fO_2–pH conditions of the fluid (Ohmoto & Goldhaber 1997). Such a model would describe trapping of externally derived hydrothermal fluids within cap-rock situations (contacts between siliceous limestones and black shales) of the Arnsberg anticline, resulting in stibnite deposition from a relatively limited batch of fluid. To test the effect of such closed-system fractionation, a Rayleigh model has been applied to our sulphur isotope dataset, choosing a temperature of 200 °C and a starting fluid composition of −18.0‰, which represents the composition of H_2S in equilibrium with the most negative $\delta^{34}S$ value of Arnsberg stibnite (−21.3‰). The Rayleigh fractionation results in a progressive shift of the stibnite composition to more positive (less negative) $\delta^{34}S$ values with time (Fig. 7). Precipitation of a relatively large molar fraction (0.99) of the initial fluid H_2S sulphur as stibnite is required to explain the compositional variation of the Arnsberg antimony mineralization. The relative direction of isotopic evolution in an extensional fibrous stibnite vein (margin: −21.0‰, centre: −20.3‰; sample BOC-1, Table 2) is essentially consistent with fluid evolution via Rayleigh fractionation. A similar

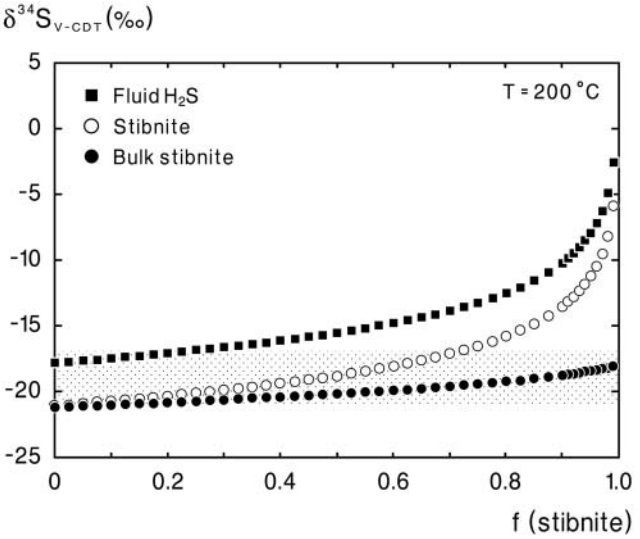

Fig. 7. Results of Rayleigh fractionation modelling for stibnite precipitation from a H_2S-fluid having a $\delta^{34}S$ value of −18.0‰ at a temperature of 200 °C. The compositional range of stibnite from the Arnsberg antimony mineralization is shown as a shaded field.

relationship cannot be established for the stibnite impregnations in black shales; the detected variation of the $\delta^{34}S$ values in the range of −20.8‰ to −17.1‰ is not correlated with the relative textural or temporal evolution. Considering the relationships between compositional and textural variation of the antimony mineralization styles, we conclude that Rayleigh fractionation was not the dominant factor controlling the sulphur isotope composition of the deposited stibnite.

fO_2–pH variations

The effect of variations of the fO_2–pH conditions, which can cause strong shifts of the isotopic composition of sulphide minerals (Ohmoto & Goldhaber 1997), appears to have been of minor importance. On an fO_2–pH diagram (constructed at 200 °C, saturated water vapour pressure and $\Sigma aS = 0.01$) for the system Fe–Sb–S–O–H (Williams-Jones & Normand 1997), the upper limit of the stibnite stability field is located very close to the predominance boundary between reduced and oxidized sulphur species, where strong fractionation of S isotopes can occur (Fig. 8). Most of the stibnite field lies in the area of predominance of the H_2S (aq) and HS^- species, where isotopic fractionation between fluid and precipitated sulphide minerals is insignificant. The conditions of mineral precipitation at the Arnsberg deposit can be further constrained using the Fe content in sphalerite (0.2–0.5 wt%), which allows calculation of aS_2 (equation from Scott & Barnes 1971) and, subsequently, of fO_2 from equilibria involving S_2 and the various aqueous S species. The fO_2 conditions established from these calculations are below the boundary between oxidized and reduced sulphur species. Similarly, the variation of sulphur isotope composition in stibnite is not correlated with the temporal evolution of the quartz–stibnite veinlets. A systematic shift of the $\delta^{34}S$ values of stibnite with time (i.e. along the growth direction) would be expected for a fluid evolution trend crossing the boundary between oxidized and reduced sulphur species. Different growth zones of fibrous stibnite veins show only very small isotopic variations and zinkenite, which has been deposited subsequent to stibnite, has a range of $\delta^{34}S$ values essentially identical to that of the stibnite. Based on the dataset and the evaluation of various processes in the depositional environment, it is clear that the sulphur isotope composition of the hydrothermal fluids responsible for stibnite mineralization has not been significantly modified during fluid evolution. Taking into account the isotopic fractionation between stibnite and fluid H_2S, we consider the $\delta^{34}S$ values of the studied antimony mineralization styles as more or less characteristic of the fluid source.

Sedimentary pyrite

Compared with the $\delta^{34}S$ values of the various styles of stibnite mineralization, sedimentary–diagenetic pyrites of the host-rock black shales and bituminous limestones are characterized by a very large compositional variation. Most of the pyrite $\delta^{34}S$ values lie outside the range of the stibnites, but several large pyrite crystals have a composition similar to the stibnite (Fig. 6). Considering the equilibrium sulphur isotope fractionation between pyrite and stibnite (Δ_{py-st}), which is in the range of 4.6–6.3‰ in the temperature interval 220–150 °C, the compositional overlap between black shale pyrites and stibnite mineralization becomes significantly broader. Detailed sulphur isotope investigation has demonstrated that bulk pyrite concentrates from a variety of Lower Carboniferous black shales and other C_{org}-rich sediments in the area possess a considerable compositional range

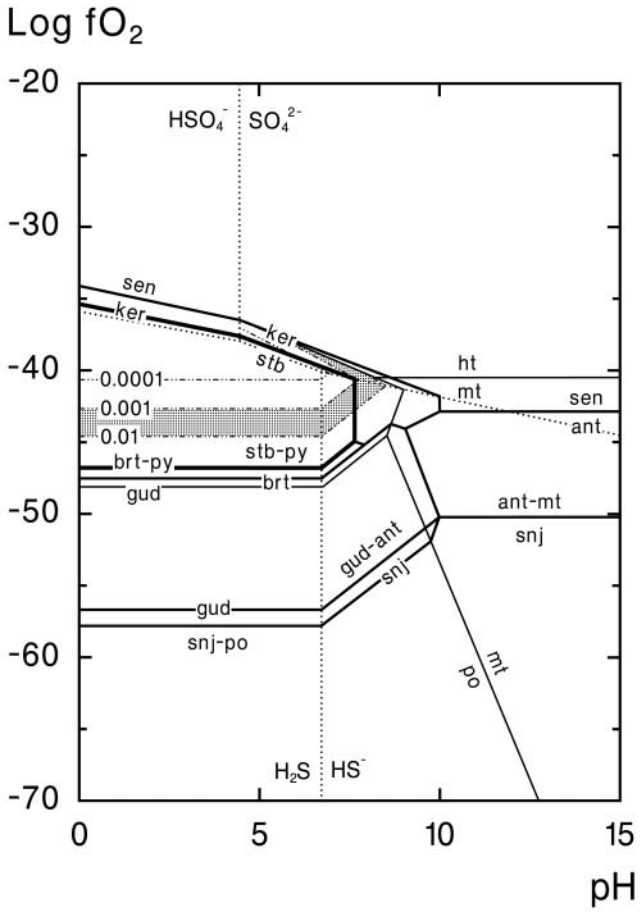

Fig. 8. Log fO_2–pH diagram at 200 °C and $\Sigma aS = 0.01$, showing stability relationships in the system Fe–Sb–S–O–H (Williams-Jones & Normand 1997) and sphalerite isopleths within the pyrite stability field (Scott & Barnes 1971). The shaded area indicates the compositional field of sphalerite from the Arnsberg stibnite veins. stb, stibnite; ant, native antimony; gud, gudmundite; brt, berthierite; snj, seinäjokite; ker, kermesite; sen, senarmontite; py, pyrite; po, pyrrhotite; mt, magnetite; ht, hematite.

of −45.4‰ to +0.8‰ (Koch 1993). This compositional field is significantly larger than the range established from our analyses, which may be related to the dominant pyrite grain sizes analysed in either study. Laser combustion analysis, which provides excellent textural resolution, is necessarily restricted to grains larger than 100 μm on average, whereas analysis of bulk pyrite concentrates includes both coarse and fine grain fractions. The smaller grain size fractions of pyrite tend to form during the early diagenetic stage under conditions of fully open-system sulphate reduction, whereas larger crystals and aggregates commonly form during late diagenesis in a more or less closed system (e.g. Canfield & Raiswell 1991; Ohmoto & Goldhaber 1997). This results in generally more negative $\delta^{34}S$ values of the finer grain fractions, and an increase in $\delta^{34}S$ with evolving texture.

Given the large range of pyrite $\delta^{34}S$ values in the various black shales and bituminous limestones in the studied area, it appears improbable that very local source rocks could have supplied the sulphur for the stibnite mineralizations. The sulphur isotope effect of fluid–rock interaction processes appears not to have been pronounced, because replacement of black shale pyrite by stibnite has not been detected and the sulphur isotope

composition of pyrite in direct association with Sb mineralization is distinctly different from that of the stibnite. This is rather obvious in the sample BOC-3, where framboidal sedimentary pyrite has a $\delta^{34}S$ value of −4.0‰, whereas stibnite shows distinctly different $\delta^{34}S$ of −20.8‰ and −17.1‰. The observed compositional homogeneity of the stibnites, irrespective of different structural and textural features, points to the influx of sulphur from a particularly well-mixed external fluid.

A Givetian source?

A potential rock source could have been Middle Devonian (Givetian) slates, which are exposed in a tectonostratigraphic unit SE of the mineralized areas. The sulphur isotope compositions of pyrites from these pelites show a relatively narrow range in composition with $\delta^{34}S$ of −28.2‰ to −7.5‰ (Koch 1993), and a mean composition of -17.1 ± 7.2‰ (1σ), which is very close to the value of H_2S in equilibrium with the stibnite (Fig. 6d). Derivation of the fluids responsible for antimony mineralization from the Middle Devonian slates is also consistent with the tectonometamorphic setting of the study area. The Middle Devonian pelites, which could have supplied the mineralizing fluids, are situated in a synclinal structure, which has been extensively overthrust by a major overturned anticline (the Sauerland main anticline) during the late stage of Variscan compressional tectonics (Weber 1977; Bauer *et al*. 1979). The overthrusting might have induced the expulsion of hydrothermal fluids from the pelite sequences and large-scale fluid movements towards the northern margin of the orogen. The expelled hydrothermal fluids were trapped in cap-rock situations inside anticlinal zones, such as the major lithological contrast between siliceous limestones and black shales at the flanks of the Arnsberg anticline. This resulted in significant cooling of the hydrothermal fluids and the deposition of stibnite and minor amounts of sulphosalt minerals (Wagner & Cook 2000).

This model might similarly explain why vein-type antimony mineralizations in other parts of the Rhenish Massif, notably sulphosalt-rich fissure veins of the Ramsbeck Pb–Zn deposit, do not display comparable negative $\delta^{34}S$ values (Wagner & Boyce 2001a, 2001b). These deposits are all located SE of the Givetian pelite-rich sedimentary sequences and are structurally related to major crustal-scale thrust zones, which have focused the syn- and late-orogenic fluid flow. Formation of most of the antimony veins in the Rhenish Massif can therefore be related to large-scale movement of deep-sourced metamorphogenic fluids along major crustal-scale discontinuities. An analogous pattern of palaeofluid migration has already been proposed for a widespread type of synorogenic Pb–Zn veins in the Rhenish Massif, based on fluid inclusion analysis, REE geochemistry and stable isotope data (Behr *et al*. 1993; Hein 1993). The ultimate source rocks supplying both the metals and sulphur of these mineralizations remain speculative, because they are not exposed on the surface. Our model of a more lateral-directed fluid flow at the northern margin of the Rhenish Massif is in accordance with the results of regional mineralogical–geochemical studies of synorogenic mineralization and Variscan fluid regimes in the Ardennes and the northern foreland of the Variscan orogen (e.g. Muchez *et al*. 1998, 2000; Kenis *et al*. 2000; Schroyen & Muchez 2000).

Conclusions

(1) The sulphur isotope composition of the Arnsberg stibnite–sulphosalt mineralization shows a very narrow range, with a mean of -20.1 ± 1.8‰ (1σ). There is no evidence for significant modification of the hydrothermal fluid source during deposition, thus measured mineral values are probably a close reflection of the fluid $\delta^{34}S$.

(2) In contrast, sedimentary–diagenetic pyrites in various local and regional Carboniferous black shales and bituminous limestones display a large variation of their $\delta^{34}S$ between −45.4‰ and +9.3‰, based on a compilation of published and our new data.

(3) The sulphur isotope characteristics of the stibnite mineralization sharply contrast with those of local sedimentary units, suggesting that the local units did not provide sulphur for the Arnsberg stibnite deposits.

(4) We propose a model involving the leaching and isotopic homogenization of sulphur from Middle Devonian shales. The $\delta^{34}S$ values of pyrite in these shales (−28.2‰ to −7.5‰; mean −17.1‰) display a significantly more narrow range than do the Carboniferous units. In addition, the pyrites from Middle Devonian shales closely match the $\delta^{34}S$ values of the Arnsberg stibnite deposits.

(5) Our study indicates northward, crustal-scale (10–20 km) lateral movement of hydrothermal fluids, consistent with observations in other parts of the northern margin of the Variscan orogen.

P. Spaethe (University of Würzburg) is thanked for the preparation of polished sections carried out in excellent quality. The assistance of T. Donnelly, J. Dougans, A. Tait and C. Taylor during S isotope analyses was much appreciated. SUERC is funded by NERC and the consortium of Scottish universities. A.J.B. is funded by NERC support of the Isotope Community Support Facility at SUERC. We thank S. Bottrell and E. Ripley for their considered reviews, which improved this contribution.

References

Ahrendt, H., Clauer, N., Hunziker, J.C. & Weber, K. 1983. Migration of folding and metamorphism in the Rheinisches Schiefergebirge deduced from K–Ar and Rb–Sr age determinations. *In:* Martin, H. & Eder, F.W. (eds) *Intracontinental Fold Belts*. Springer, Berlin, 323–339.

Arias, D., Corretgé, L.G., Villa, L., Gallastegui, G., Suárez, O. & Cuesta, A. 1997. A sulphur isotopic study of the Navia gold belt (Spain). *Journal of Geochememical Exploration*, **59**, 1–10.

Arthaud, F. & Matte, P. 1977. Late Paleozoic strike-slip faulting in southern Europe and northern Africa: result of a right-lateral shear zone between the Appalachians and the Urals. *Geological Society of America Bulletin*, **88**, 1305–1320.

Barker, A.J., Bennett, D.G., Boyce, A.J. & Fallick, A.E. 2000. Retrogression by deep infiltration of meteoric fluids into thrust zones during late-orogenic rapid unroofing. *Journal of Metamorphic Geology*, **18**, 307–318.

Bauer, G. & Ebert, A. *et al*. 1979. Die Blei–Zink-Erzlagerstätten von Ramsbeck und Umgebung. *Geologisches Jahrbuch*, D33.

Behr, H.J., Gerler, J., Hein, U.F. & Reutel, C.J. 1993. Tectonic Brines und Basement Brines in den mitteleuropäischen Varisziden: Herkunft, metallogenetische Bedeutung und geologische Aktivität. *Göttinger Arbeiten zur Geologie und Paläontologie*, **58**, 3–28.

Bierlein, F.P. & Crowe, D.E. 2000. Phanerozoic orogenic lode gold deposits. *Reviews in Economic Geology*, **13**, 103–139.

Boiron, M.C., Cathelineau, M., Dubessy, J. & Bastoul, A.M. 1990. Fluids in Hercynian Au veins from the French Variscan belt. *Mineralogical Magazine*, **54**, 231–243.

Bottrell, S.H. & Spiro, B. 1988. A stable isotope study of black shale-hosted gold mineralization in the Dolgellau Gold Belt, North Wales. *Journal of the Geological Society, London*, **145**, 941–949.

Bottrell, S.H., Shepherd, T.J., Yardley, B.W.D. & Dubessy, J. 1988. A fluid inclusion model for the genesis of the ores of the Dolgellau Gold Belt, North Wales. *Journal of the Geological Society, London*, **145**, 139–145.

Büker, C., Littke, R. & Welte, D.H. 1995. 2D-modelling of the thermal evolution of Carboniferous and Devonian sedimentary rocks of the eastern Ruhr basin and northern Rhenish Massif, Germany. *Zeitschrift der Deutschen Geologischen Gesellschaft*, **146**, 321–339.

Canfield, D.E. & Raiswell, R. 1991. Pyrite formation and fossil preservation. *In:* Allison, P.A. & Briggs, D.E.G. (eds) *Taphonomy: Releasing the Data Locked in the Fossil Record*. Plenum, New York, 337–387.

Clausen, C.D. 1984. *Erläuterungen zur geologischen Karte von Nordrhein-Westfalen 1:25 000, Blatt 4515 Hirschberg*. Geologisches Landesamt Nordr-

hein-Westfalen, Krefeld.

Clausen, C.D. & Leuteritz, K. 1984. *Erläuterungen zur geologischen Karte von Nordrhein-Westfalen 1:25000, Blatt 4516 Warstein*. Geologisches Landesamt Nordrhein-Westfalen, Krefeld.

Clausen, C.D., von Kamp, H., *et al.* 1981. *Erläuterungen zur geologischen Karte von Nordrhein-Westfalen 1:100 000, Blatt C4714 Arnsberg*. Geologisches Landesamt Nordrhein-Westfalen, Krefeld.

Clayton, R.E. & Spiro, B. 2000. Sulphur, carbon and oxygen isotope studies of early Variscan mineralisation and Pb–Sb vein deposits in the Cornubian orefield: implications for the scale of fluid movements during Variscan deformation. *Mineralium Deposita*, **35**, 315–331.

Cox, S.F., Etheridge, M.A. & Wall, V.J. 1986. The role of fluids in syntectonic mass transport, and the localization of metamorphic vein-type ore deposits. *Ore Geology Reviews*, **2**, 65–86.

Dill, H.G. 1985. Antimoniferous mineralization from the Mid-European Saxothuringian Zone: mineralogy, geology, geochemistry and ensialic origin. *Geologische Rundschau*, **74**, 447–466.

Dill, H.G. 1998. Evolution of Sb mineralisation in modern fold belts: a comparison of the Sb mineralisation in the Central Andes (Bolivia) and the Western Carpathians (Slovakia). *Mineralium Deposita*, **33**, 359–378.

Dittmar, U., Meyer, W., Oncken, O., Schievenbusch, T., Walter, R. & von Winterfeld, C. 1994. Strain partitioning across a fold and thrust belt: the Rhenish Massif, Mid-European Variscides. *Journal of Structural Geology*, **16**, 1335–1352.

Fallick, A.E., McConville, P., Boyce, A.J., Burgess, R. & Kelley, S.P. 1992. Laser microprobe stable isotope measurements on geological materials: some experimental considerations (with special reference to (^{34}S in sulphides). *Chemical Geology*, **101**, 53–61.

Franke, W. & Oncken, O. 1990. Geodynamic evolution of the North–Central Variscides—a comic strip. *In:* Freeman, R., Giese, P. & Mueller, S. (eds) *The European Geotraverse: Integrative Studies*. European Science Foundation, Strasbourg, 187–194.

Gray, D.R., Gregory, R.T. & Durney, D.W. 1991. Rock-buffered fluid–rock interaction in deformed quartz-rich turbidite sequences, eastern Australia. *Journal of Geophysical Research*, **96**, 19681–19704.

Guillemette, N. & Williams-Jones, A.E. 1993. Genesis of the Sb–W–Au deposits at Ixtahuacan, Guatemala: evidence from fluid inclusions and stable isotopes. *Mineralium Deposita*, **28**, 167–180.

Gumiel, P. & Arribas, A. 1987. Antimony deposits in the Iberian Peninsula. *Economic Geology*, **82**, 1453–1463.

Hein, U.F. 1993. Synmetamorphic Variscan siderite mineralization of the Rhenish Massif, Central Europe. *Mineralogical Magazine*, **57**, 451–467.

Heinrich, C.A., Andrew, A.S. & Knill, M.D. 2000. Regional metamorphism and ore formation: evidence from stable isotopes and other fluid tracers. *Reviews in Economic Geology*, **11**, 97–117.

Henk, A. 1995. Late Variscan exhumation histories of the southern Rhenohercynian zone and western Mid-German Crystalline Rise: results from thermal modelling. *Geologische Rundschau*, **84**, 578–590.

Kelley, S.P. & Fallick, A.E. 1990. High precision spatially resolved analysis of (^{34}S in sulphides using a laser extraction technique. *Geochimica et Cosmochimica Acta*, **54**, 883–888.

Kenis, I., Muchez, P., Sintubin, M., Mansy, J.L. & Lacquement, F. 2000. The use of a combined structural, stable isotope and fluid inclusion study to constrain the kinematic history at the northern Variscan front zone (Bettrechies, northern France). *Journal of Structural Geology*, **22**, 589–602.

Koch, H.P. 1993. *Sulfidgenese in Sedimenten des Rheinischen Schiefergebirges*PhD Thesis, University of Göttingen.

Kühne, F. 1938a. *Erläuterungen zur geologischen Karte von Preußen und benachbarten deutschen Ländern 1:25 000, Blatt 4514 Arnsberg-Nord.* Preußische Geologische Landesanstalt, Berlin.

Kühne, F. 1938b. *Erläuterungen zur geologischen Karte von Preußen und benachbarten deutschen Ländern 1:25 000, Blatt 4614 Arnsberg-Süd*. Preußische Geologische Landesanstalt, Berlin.

Muchez, P., Zhang, Y., Dejonghe, L., Viaene, W. & Keppens, E. 1998. Evolution of palaeofluids at the Variscan thrust front in eastern Belgium. *Geologische Rundschau*, **87**, 373–380.

Muchez, P., Sintubin, M. & Swennen, R. 2000. Origin and migration of palaeofluids during orogeny: discussion on the Variscides of Belgium and northern France. *Journal of Geochemical Exploration*, **69-70**, 47–51.

Mullis, J., Dubessy, J., Poty, B. & O'Neil, J. 1994. Fluid regimes during late stages of a continental collision: physical, chemical, and stable isotope measurements of fluid inclusions in fissure quartz from a geotraverse through the Central Alps, Switzerland. *Geochimica et Cosmochimica Acta*, **58**, 2239–2267.

Munoz, M., Courjault-Radé, P. & Tollon, F. 1992. The massive stibnite veins of the French Paleozoic basement: a metallogenic marker of Late Variscan brittle extension. *Terra Nova*, **4**, 171–177.

Nesbitt, B.E., Muehlenbachs, K. & Murowchick, J.B. 1989. Genetic implications of stable isotope characteristics of mesothermal Au deposits and related Sb and Hg deposits in the Canadian Cordillera. *Economic Geology*, **84**, 1489–1506.

Noronha, F. & Cathelineau, M. *et al.* 2000. A three stage fluid flow model for Variscan gold metallogenesis in northern Portugal. *Journal of Geochemical Exploration*, **71**, 209–224.

Ohmoto, H. 1972. Systematics of sulfur and carbon isotopes in hydrothermal ore deposits. *Economic Geology*, **67**, 551–578.

Ohmoto, H. & Goldhaber, M.B. 1997. Sulfur and carbon isotopes. *In:* Barnes, H.L. (ed.) *Geochemistry of Hydrothermal Ore Deposits*, *3rd edition*. Wiley, New York, 517–611.

Ohmoto, H. & Rye, R.O. 1979. Isotopes of sulfur and carbon. *In:* Barnes, H.L. (ed.) *Geochemistry of Hydrothermal Ore Deposits*, *2nd edition*. Wiley, New York, 509–567.

Oliver, N.H. & Bons, P.D. 2001. Mechanisms of fluid flow and fluid–rock interaction in fossil metamorphic hydrothermal systems inferred from vein–wallrock patterns, geometry and microstructure. *Geofluids*, **1**, 137–162.

Oncken, O. 1984. Zusammenhänge in der Strukturgenese des Rheinischen Schiefergebirges. *Geologische Rundschau*, **73**, 619–649.

Oncken, O. 1988. Aspects of the reconstruction of the stress history of a fold and thrust belt (Rhenish Massif, Federal Republic of Germany). *Tectonophysics*, **152**, 19–40.

Oncken, O. 1991. Aspects of the structural and paleogeothermal evolution of the Rhenish Massif. *Annales de Societe Géologique Belgique*, **113**, 139–159.

Ortega, L. & Vindel, E. 1995. Evolution of ore-forming fluid associated with late Hercynian antimony deposits in Central/Western Spain: case study of Mari Rosa and El Juncalón. *European Journal of Mineralogy*, **7**, 655–673.

Partington, G.A. & Williams, P.J. 2000. Proterozoic lode gold and (iron)–copper–gold deposits: a comparison of Australian and global examples. *Reviews in Economic Geology*, **13**, 69–101.

Pettke, T. & Diamond, L.W. 1997. Oligocene gold quartz veins at Brusson, NW Alps: Sr isotopes trace the source of ore-bearing fluid to over a 10-km depth. *Economic Geology*, **92**, 389–406.

Pettke, T., Diamond, L.W. & Villa, I.M. 1999. Mesothermal gold veins and metamorphic devolatilization in the northwestern Alps: the temporal link. *Geology*, **27**, 641–644.

Ramsay, J.G. & Huber, M.I. 1987. *The Techniques of Modern Structural Geology.* Academic Press, London, **2**.

Robinson, B.W. & Kusakabe, M. 1975. Quantitative preparation of sulfur dioxide for ^{34}S/^{32}S analyses from sulphides by combustion with cuprous oxide. *Analytical Chemistry*, **47**, 1179–1181.

Rye, R.O. 1993. The evolution of magmatic fluids in the epithermal environment: the stable isotope perspective. *Economic Geology*, **88**, 733–753.

Schroyen, K. & Muchez, P. 2000. Evolution of metamorphic fluids at the Variscan fold-and-thrust belt in eastern Belgium. *Sedimentary Geology*, **131**, 163–180.

Scott, S.D. & Barnes, H.L. 1971. Sphalerite geothermometry and geobarometry. *Economic Geology*, **66**, 466–474.

Tosdal, R.M., Wooden, J.L. & Bouse, R.M. 1999. Pb isotopes, ore deposits, and metallogenic terranes. *Reviews in Economic Geology*, **12**, 1–28.

Wagner, T. & Boyce, A.J. 2001a. Sulphur isotope characteristics of recrystallisation, remobilisation and reaction processes: a case study from the Ramsbeck Pb–Zn, Germany. *Mineralium Deposita*, **36**, 670–679.

Wagner, T. & Boyce, A.J. *et al.* 2001b. Sulphide–sulphosalt reactions and sphalerite remobilization in siderite–Pb–Zn–Sb veins of the Siegerland district, Germany: a laser microprobe sulphur isotope study. *In:* Piestrzynski, A. (ed.) *Mineral Deposits at the Beginning of the 21st Century. Proceedings of the Joint 6th Biennial SGA–SEG meeting, Krakow.* Balkena, Rotterdam, 185–188.

Wagner, T. & Cook, N.J. 2000. Late-Variscan antimony mineralization in the Rheinisches Schiefergebirge, NW Germany: evidence for stibnite precipitation by drastic cooling of high-temperature fluid systems. *Mineralium Deposita*, **35**, 206–222.

Wagner, T., Boyce, A.J. & Fallick, A.E. 2002. Laser combustion analysis of δ^{34}S of sulfosalt minerals: determination of the fractionation systematics and some crystal-chemical considerations. *Geochimica et Cosmochimica Acta*, **66**, 2855–2863.

Weber, K. 1977. Bau und tektonische Entwicklung des Ostsauerländer Hauptsattels und der varistischen Ramsbecker Blei–Zinkerzlagerstätte. *Fortschritte der Mineralogie*, **55**, 48–63.

Williams-Jones, A.E. & Normand, C. 1997. Controls of mineral parageneses in the system Fe–Sb–S–O. *Economic Geology*, **92**, 308–324.

Received 30 January 2002; revised typescript accepted 19 September 2002.
Scientific editing by Anthony Cohen